Journal of Natural Gas Science and Engineering 107 (2022) 104768

Contents lists available at ScienceDirect

Journal of Natural Gas Science and Engineering

journal homepage: www.elsevier.com/locate/jngse

Evaluating essential features of proppant transport at engineering scales combining field measurements with machine learning algorithms

Lei Hou [a,*], Xiaoyu Wang [b,**], Xiaobing Bian [c], Honglei Liu [c], Peibin Gong [d]

[a] School of Engineering, The University of Warwick, Coventry, CV4 7AL, UK
[b] Institute for Building Materials, ETH Zurich, Zurich, 8049, Switzerland
[c] SINOPEC Research Institute of Petroleum Engineering, Beijing, 100101, China
[d] Drilling Technology Research Institute of SINOPEC, Shengli Oilfield Service Corporation, Dongying, 257017, China

ARTICLE INFO

Keywords:
Proppant transport
Feature evaluation
Machine learning
Pressure variation
Field scales

ABSTRACT

The behaviours of the particle settlement, stratified flow and inception of settled particles are essential features that determine the proppant transport in low-viscosity fracturing fluids. Although great efforts have been made to characterize these features, limited research work is performed at field scales. To test the laboratory outcomes, we propose a machine-learning-based workflow to evaluate the essential features using the measurements obtained from shale gas fracturing wells. Over 430,000 groups of fracturing data (1 s time interval) are collected and pre-processed to extract the particle settlement, stratified flow and inception features during fracturing operations. The GRU and SVM algorithms, trained by these features, are applied to predict fracturing pressure. Error analysis (the root mean squared error, RMSE) is carried out to compare the contributions of different features to the pressure prediction, based on which the features and the corresponding calculations are evaluated. Our result shows that the stratified-flow feature (fracture-level) possesses better interpretations for the proppant transport, in which the Bi-power model helps to produce the best predictions. The settlement and inception features (particle-level) perform better in cases where the pressure fluctuates significantly. The features characterize the state of proppant transport, based on which the development of subsurface fracture is also analyzed. Moreover, our analyses of the remaining errors in the pressure-ascending cases suggest that (1) an introduction of the alternate-injection process, and (2) the improved calculation of proppant transport in highly-filled fractures will be beneficial to both experimental observations and field applications.

1. Introduction

Hydraulic fracturing has become an important technique to enhance hydrocarbon recovery from unconventional gas resources, aiming to meet the growing demand for clean energy globally. To avoid fracture closure after the dissipation of the hydraulic injecting pressure, proppant injections are essential in the hydraulic fracturing process, and their effectiveness plays an important role in enhancing the stimulated reservoir volume (Barree and Conway, 1994; L. Fan, Thompson and Robinson, 2010; Nassir et al., 2014). To inject thousands of tons of proppant particles down into the induced fractures, a deep well in a shale gas reservoir (>4000 m) is usually operated under a wellhead pressure exceeding 100 MPa (Hou, Chang, Fu, Muhadasi and Chen, 2019a, 2019b; Mao et al., 2021). Therefore, how to inject proppant particles under safe operating pressures is very challenging, especially with the application of low-viscosity slickwater (Liang et al., 2016). Proppant transport is, therefore, an essential research topic in hydraulic fracturing engineering (Economides and Nolte, 1989).

The behaviours of the proppant settlement, stratified flow and inception of settled particles in low-viscosity fracturing fluid have been characterized numerically based on experimental tests (Gadde et al., 2004; Wei et al., 2020; Zhao et al., 2019), which are the essential features of proppant transport. The recent trend of the proppant transport research is to bring in more realistic subsurface scenarios by replacing the single smooth-panel fracture with artificial-coarse fracture networks (Manchanda et al., 2020; Raki Sahai and Moghanloo, 2019; Tong and Mohanty, 2016). However, it is still challenging to simulate and characterize the realistic morphology (scale, tortuosity, branches et al.) of

* Corresponding author.
** Corresponding author.
E-mail addresses: leihou.upc@gmail.com (L. Hou), xiaoyu.wang@ifb.baug.ethz.ch (X. Wang).

https://doi.org/10.1016/j.jngse.2022.104768
Received 23 January 2022; Received in revised form 4 August 2022; Accepted 20 August 2022
Available online 28 August 2022
1875-5100/© 2022 The Authors. Published by Elsevier B.V. This is an open access article under the CC BY license (http://creativecommons.org/licenses/by/4.0/).

fractures numerically (Dahi-Taleghani and Olson, 2011). Moreover, the direct subsurface measurements and observations during fracturing operations are still limited. Many numerical models for calculating the proppant transport, therefore, are usually verified by laboratory experiments (Mack et al., 2014; Patankar et al., 2002; Raki Sahai and Moghanloo, 2019). However, the approaches for examining the numerical observations at a field scale are still in demand.

The links between indoor research and field practice may rely on exploring the key property features that control the proppant transports (Cai et al., 2017). Machine learning (ML) is one of the key techniques to perform the exploration at field-practical scales. Researchers built ML workflows to predict the fracturing pressure and forewarn the sand screen-out in real-time based on fracturing records (Ben et al., 2020; Hu et al., 2020). The simulation data is also applied to learn the pressure pattern and detect sand screen-out (Yu et al., 2020). These effects help to improve the safety of fracturing operations by combining data science and engineering knowledge. It is also important to understand how the key features, being tested in the lab, influent the proppant transport during real fracturing operations, which may, in turn, promote fundamental research.

In this study, we examine and compare essential features of proppant transport and their corresponding calculations by using a new workflow, where we introduce machine learning (ML) algorithms, including Support Vector Regression (Al-Anazi and Gates, 2010; Al-Mudhafar, 2017) and Gated Recurrent Units (L. Hou, Cheng, Wang, Ren and Geng, 2022; Sun et al., 2020). The ML method can process the field measurements for proppant transport evaluation directly without in-depth characteristics of the realistic fracture morphology, which may build a bridge between the fundamental research and field applications. Based on the data-driven approach, our study is aimed to 1) propose a new workflow to estimate the proppant transport at field engineering scales; and 2) better understand the essential features that control the proppant transport, which is valuable for both field engineering and basic research work.

2. Methodology

The field measurements of the shale gas fracturing treatments are collected and carefully pre-processed (splitting, trimming, and denoising) for training. The proppant transport features, specifically the velocity ratio and the height of the flowing layers within fractures, are initially calculated by several popular proppant transport models. The calculation outputs consisting of the features relevant to the proppant flow, as long as the other subsurface measurements, are then fed into the machine learning algorithms to predict downhole pressure. The predictions are further analyzed using the control variate method and error analyses to evaluate the proppant transport features and their corresponding calculations.

2.1. Data collection and preprocessing

55 stages, including over 430,000 groups, of fracturing measurements (in second) are collected from 10 shale gas wells, which are selected from 5 different platforms in the Sichuan basin, China (Table 1). The field measurements include the geological data (vertical and well depths), clustering data (stage length, cluster number and perforation number), and fracturing data (fluid and proppant types, pump rate, proppant concentration and wellhead pressure). Five of the ten wells are set as the training well ($A_1 - E_1$), of which 50 stages of fracturing data are pre-processed for training the machine learning models. Five testing stages are selected from the remaining five wells ($A_2 - E_2$), defined as testing wells. To constrain the effect of large spatial variation in geological uncertainty and formation properties on the predictions, each training well has its own testing well that is selected from the same platform. For instance, both Well A_1 and Well A_2 (neighbouring wells) are from Platform A, and so forth, as shown in Table 1. This is one of our strategies to eliminate interference factors of pressure variation and promote the influence of proppant transport.

Table 1
Division of training and testing datasets.

	Platform A		Platform B		Platform C		Platform D		Platform E	
Well No.	A_1		B_1		C_1		D_1		E_1	
Training Dataset/ Stages	10	/	10	/	10	/	10	/	10	/
Well No.		A_2		B_2		C_2		D_2		E_2
Testing Dataset/ Stages	/	1	/	1	/	1	/	1	/	1

The other strategy during the data preprocessing is to convert the wellhead pressure into the downhole pressure after the perforation hole (Appendix A), defined as the DPP. The conversion can rule out the potential effects of hydrostatic pressure and friction variations, leaving the proppant transport to control the fracture pressure fluctuation (Dontsov and Peirce, 2014; Willingham et al., 1993). Other denoising methods involve trimming the pressure at the beginning (when the fracture is created) and the end (pump-off) of the fracturing operation, repeating predictions and averaging the errors obtained from all the platforms (A – E), as long as applying two different machine learning algorithms.

2.2. Features for proppant transport

In general, we divide the proppant transport features into two categories by their scales – particle level (Fig. 1 a) and fracture level (Fig. 1 b), including the particle settling velocity (Gadde et al., 2004; Mack et al., 2014; McCabe et al., 1993; Richardson and Zaki, 1954; Yew and Weng, 2014), the critical velocity to restart the settled proppant (also used as the critical turning velocity in complex fractures) (Cao et al., 2006; Hou, Jiang, Li, Zeng and Cheng, 2017a, 2017b; Hou, Jiang, Liu, et al., 2017a, 2017b; Rakshit Sahai, Miskimins, & Olson, 2014), the flowing layer height (H_1) (Hou et al., 2019a, 2019b; Novotny, 1977; Patankar et al., 2002; Jing Wang, Joseph, Patankar, Conway and Barree, 2003) and the equilibrium dune level (EDL – the dune height divided by fracture height) (Alotaibi and Miskimins, 2019). Based on the field pumping schedules, those features are further calculated by employing the Velocity, Settling, Bi-power, and EDL models to yield a group of independent variables, which is one of the inputs for ML models (Table 2). Details about the equations and their applications can be found in Appendix B.

The representative features, particle settlement ($v_{settling}/v_f$), inception ($v_{turning}/v_f$) and stratified-flow (H_1 and EDL) behaviours, are selected and tabulated in Table 2. The particle settlement and inception are grouped because they are decomposition features of particle movements in vertical and horizontal directions. The selected features in Table 2 control the proppant transport in the low-viscosity fluid, based on which more comprehensive models coupling fracture propagation, fluid leak-off, etc. are derived (Barboza et al., 2021; Isah et al., 2021). Besides, the calculations (Appendix B) for the selected features are analytical, which is more calculational effective to pre-processing our datasets (over 430, 000 groups of measurements) compared with numerical solutions. Furthermore, the models in Table 2 are mainly derived from observations of experimental simulations (Appendix B). By evaluating the calculation outputs at field-practical scales, the experimental techniques may be improved in the aspects of equipment, parameters, methodology, measurements, etc.

During the calculation, the fracture width is the only unknown parameter that is presumably set to a value of $100 \times d_{\max}$ ($d_{\max}$ is the largest diameter of injected proppant) referring to the result of slant core drilling through a stimulated shale reservoir (Elliott and Gale, 2018). For an alternate pumping schedule (injecting pure fluid and slurry alternatively), the results of the Velocity model are discrete and are all treated as zeros as pure fluid is injected. As shown in Table 2, the

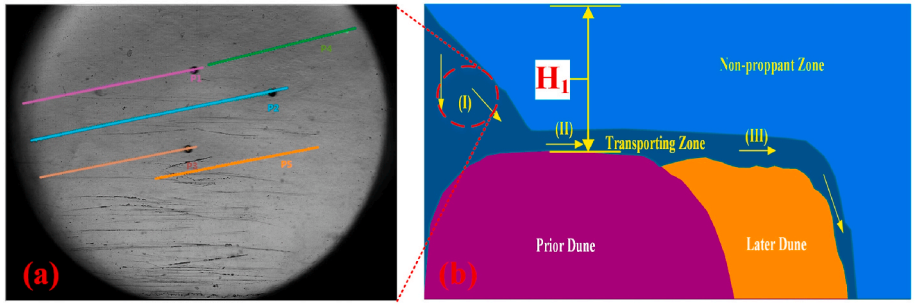

Fig. 1. Proppant transport features at (a) particle-level (particle settlement and inception); (b) fracture-level (H_1 – the height of the flowing layer) (Hou, Jiang, Liu, et al., 2017a, 2017b; Patankar et al., 2002).

Table 2
Summary of calculations, features and control variate method for data processing.

	Inputs		Output (Dependent variable)	Error analysis	Notes	
	Independent Variable (Selected features)	Control variable (field records)				
Pressure conversion	/	/	DPP (Reference)	/	/	Appendix A
Original data	/	μ, Q, C & d	DPP (without independent variable)	RMSE	For comparisons	/
Velocity model	$v_{turning}/v_f$ $v_{settling}/v_f$		DPP (with independent variable)		Derived from forces acting on particles	Appendix B
Settling model	H_1				Derived from particle settling	
Bi-power model	H_1				Derived from particle and fluid Reynold's numbers	
EDL model	EDL				Empirical model	

independent variables and the control variables (field measurements: fluid type – μ, pump rate – Q, proppant concentration – C and proppant type – d) are jointly fed into the ML models for the prediction (dependent variable: downhole pressure after perforation – DPP) and error analyses (the Root Mean Square Error – RMSE). The non-numeric variables (fluid and proppant types) are replaced with the values of fluid viscosity and averaged proppant diameters, respectively. For comparison purposes, the original field measurements alone are directly used to train the ML models to predict the DPP, defined as the unprocessed DPP (Table 2).

2.3. Machine learning models and workflow

To constrain the high variance and boost the prediction performance, two different machine learning algorithms are applied for training and predicting. The Support Vector Regression (SVR) model, with a Radial Basis Function (RBF) kernel, is capable of both linear and non-linear regression (Al-Anazi and Gates, 2010), being of memory efficiency, and performing well in various petroleum engineering applications (Goel et al., 2017; Guo et al., 2018). Furthermore, we apply Gated Recurrent Units (GRU) to the same datasets. The GRU is a deep learning algorithm designed for extracting information from time-sequence data. In GRU models, the current state and prediction can be influenced by the preceding state and will affect the following prediction at the next time step as well, making the GRU models appropriate for handling continuous hydraulic fracturing data (Sun et al., 2020; Jinjiang Wang, Yan, Li, Gao and Zhao et al., 2019). According to previous modelling experience (Cho et al., 2014; D. Fan et al., 2021), a three-layer (including the output layer) GRU model is constructed with the activation function of ReLU. The dropout (0.2) layers are applied to avoid the overfitting of the model (Gal and Ghahramani, 2015). The Adam optimizer is used in the model with a learning rate starting at 0.0005 (Kingma and Ba, 2014).

Using Platform A as an example, our workflow for the data processing is shown in Fig. 2. Model i represents one of the four proppant transport models given in Table 2. The reference is the DPP converted

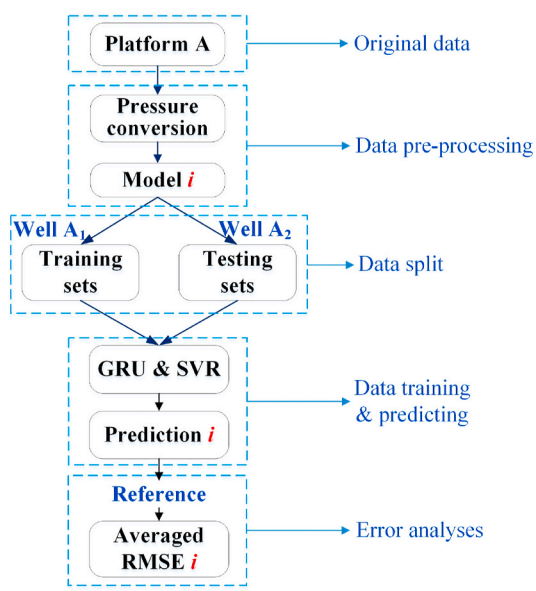

Fig. 2. Schematics of the data processing workflow using Platform A as an example.

directly from the surface pressure records, and Prediction i is the predicted DPP based on Model i. The pressure prediction is made for each platform (A to E), and for each prediction, a new GRU model and SVR model are created and trained respectively. Eventually, the prediction errors for each platform are averaged to evaluate the performance of the selected features and the corresponding models.

3. Results

3.1. Evaluation of proppant transport features at engineering scales

The pressure predictions by GRU for Well A_2 at Platform A are plotted in Fig. 3, using as an example of the evaluation results. In general, the predicted DPP curves corresponding to the proppant transport models match the reference DPP curve much better than the unprocessed curve, indicating that the introduction of the proppant transport features improves the prediction accuracy and reduces the variance (Fig. 3). The proppant concentration during the fracturing operation is also presented (green solid line in Fig. 3), demonstrating that the proppant-injection-induced pressure fluctuations influence the variation in pressure predominantly. To denoise the pressure variation induced by the injection, the pressure data ranging between the time of 2000 s (the period of the fracture initiation and propagation) and the time of 8000 s (the period of the fracture closure and fluid diffusion after pump-off) are only used for error analyses (the region between two vertical grey dash lines in Fig. 3).

Four more ML predictions are carried out for Platforms B – E. The errors based on different proppant transport models are averaged to compare the performances of the GRU and SVM algorithms, as shown in Fig. 4. Generally, the two algorithms exert close performances according to the generated errors. The GRU-based workflow produces smaller errors for Wells A_2, B_2 and C_2. Therefore, the predictions based on the GRU model are selected for further investigations. Besides, the errors for Wells A_2 and B_2 are significantly smaller than in the rest of the cases. We divided the cases into two groups in the later analyses – the small error group (Wells A_2 and B_2) and the large error group (Wells C_2, D_2, and E_2).

The detailed errors between the reference and the ML prediction for each testing well (A_2 – E_2) based on the GRU algorithm are summarized in Table 3. By comparing the averaged RMSE, we find that the DPP predictions are enhanced by introducing the Velocity, Settling, and Bi-power models, in which the stratified-flow feature performs better than the settlement and inception features. The Bi-power model helps yield the best DPP predictions, followed by the Settling model. The introduction of the EDL model promotes low RMSEs for Wells A_2, B_2, and C_2, whereas leads to large prediction errors for Wells D_2 and E_2. The performance of the Velocity model is probably limited by the simplification employed under the pure-fluid condition. However, exceptions are observed for Wells D_2 and E_2, where the Velocity model helps to produce smaller errors than the Settling model does.

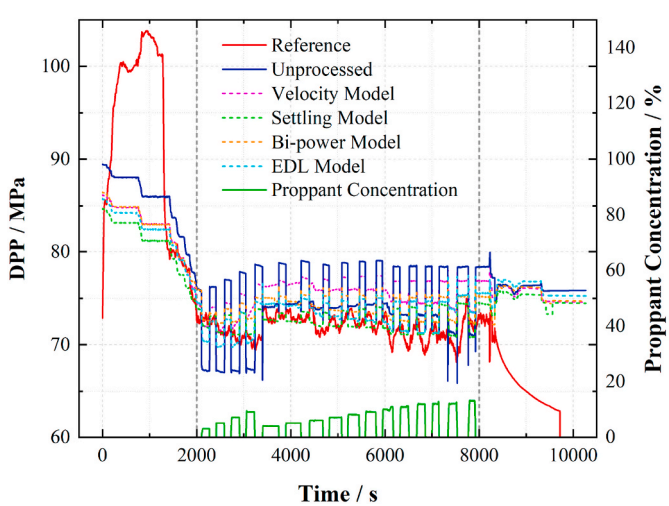

Fig. 3. Comparisons of DPP between the Reference and Predictions based on Platform A using the GRU model. The Reference curve (red solid line) is obtained by pressure conversion. The Unprocessed curve (blue solid line) is the prediction based on original injection parameters, referring to Table 2. The dashed lines are the predictions by GRU models corresponding to different proppant transport models. The green solid line is the proppant concentration.

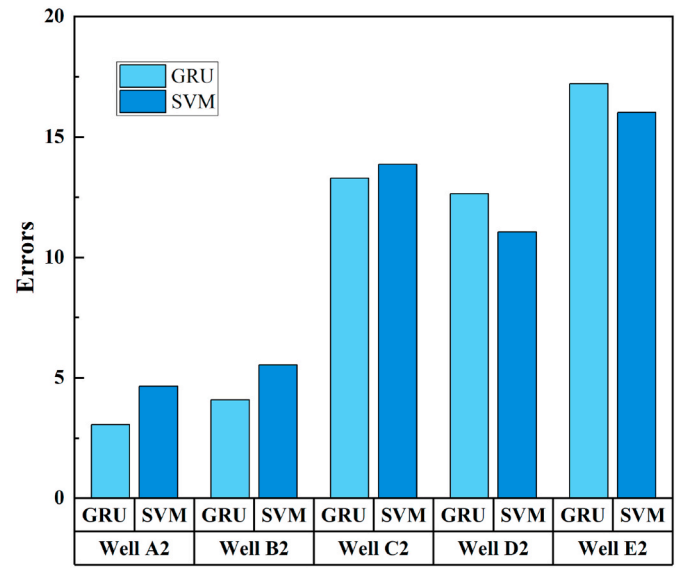

Fig. 4. The average errors produced by GRU and SVM algorithms based on Wells A_2 – E_2. Each error bar represents the averaged errors based on different proppant transport models.

3.2. Error variance in different cases

According to Table 3, we plot the DDP curves predicted by the GRU algorithm for further investigation, as shown in Figs. 5 and 6. Each dash curve corresponds to a different model used to calculate the input features, including the Velocity (particle-level feature), Settling and Bi-power (fracture-level feature) models. As the different calculations are applied for the pure-fluid and slurry injections (Appendix B) when preprocessing the input data, the predicted curves derived from the alternative injection schedule are relatively discrete. The predictions, therefore, fluctuate around the reference at a frequency following the oftenness of the injection switching.

For the small error group (Fig. 5), a relatively flat trend of DPP along with a constant pumping rate can be found throughout the injection treatment in Wells A_2 and B_2. The effect of proppant transport on pressure variation is moderate, suggesting that the fracture volume may be sufficient for the current proppant injection rate. Besides, the predicted pressure curve is unsmooth and exerts vertical climbing and jumping between slugs (the alternate from pure fracturing fluid into proppant slurry).

In contrast, an ascending pressure trend (red solid curves in Fig. 6) can be found in the large error group (Wells C_2, D_2 and E_2). Compared with the proppant concentrations in Wells A_2 and B_2 (~20%), the proppant concentrations for Well C_2, D_2, and E_2 are all under 10%, indicating that their DPPs are relatively sensitive to the proppant transport. In Well C_2, D_2, and E_2, the proppant particles are likely driven into fractures possessing insufficient volume, where the continuously injected proppant may accumulate, and then block the flowing pass (as shown in Fig. 7), resulting in a gradual increase in flowing friction, reflected by the ascending operation pressure (Zhang et al., 2017). Besides, the performance of the Velocity model is unexpected and even better than the Settling and Bi-power models, as shown in Fig. 6 (b) and (c). Integrating the severe fluctuations of fracturing pressure into account, the underground fracture in Fig. 6 may be more complex than that in Fig. 5. The proppant may be transported in fracture networks. Therefore, the Velocity model, calculating the critical condition of proppant turning from the main fracture into the minor fracture, produces better predictions.

Table 3
Summary of the RMSE based on each proppant transport model.

	Well A_2	Well B_2	Well C_2	Well D_2	Well E_2	Averaged RMSE
Algorithms	GRU	GRU	GRU	GRU	GRU	
Unprocessed	4.61	4.39	14.2	8.43	15.92	**9.51**
Velocity model	4.09	4.08	13.37	6.98	14.32	**8.57**
Settling model	1.72	4.02	12.71	9.53	14.55	**8.51**
Bi-power model	2.59	4.25	12.65	8.35	11.9	**7.95**
EDL model	2.31	3.65	13.53	29.92	29.32	**15.75**

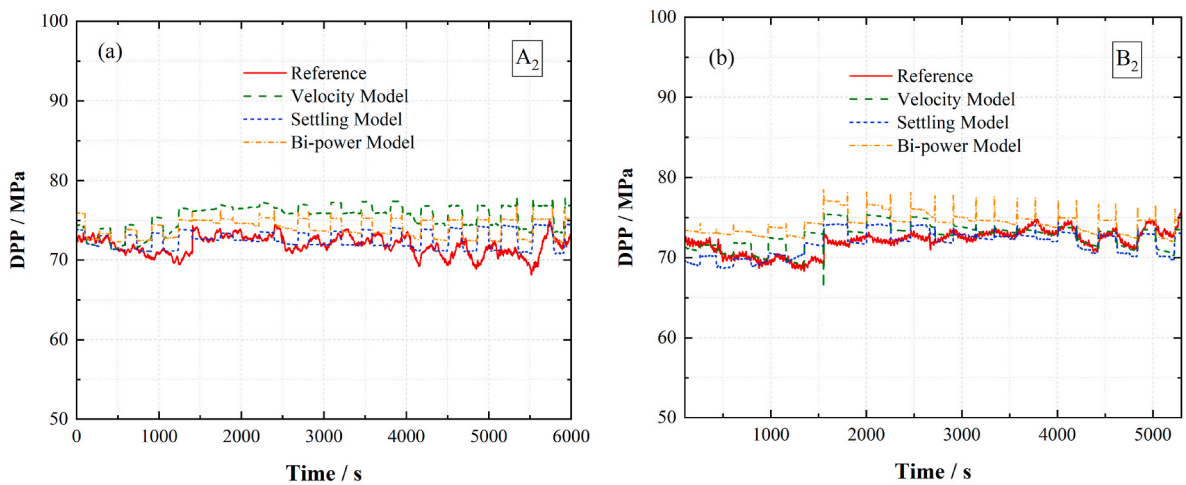

Fig. 5. Comparisons of the pressure evolution based on (a) Well A_2 and (b) Well B_2 using the GRU algorithm. The Reference curve (red solid line) is obtained by pressure conversion. The dashed lines are the proppant-transport-model-based predictions.

4. Discussion

Our comparison among pressure predictions derived from different proppant transport features exhibits that the stratified-flow feature (H_1, calculated by the Bi-power and Settling models) can improve the pressure prediction considerably. The unstable predictions produced by the EDL model may be attributed to the limited application range of the empirical equations used in the model (Appendix B). The Velocity model characterizes the particle flowing feature during the slurry injection but fails to take into account the scenario when the pure fluid is injected, which results in a restrained improvement in the pressure prediction.

However, relatively large prediction errors exist for cases of Wells C_2, D_2, and E_2 (Fig. 6), which are non-negligible and likely attributed to the following factors:

(i) Effect of the injection alternation – The proppant transport models are featured by taking into account the accumulation of the proppant dune being in an equilibrium state. Hence, the prediction curves in Figs. 5 and 6 are relatively discrete under an alternate injection schedule. However, the time interval (around 3–5 min) between the injecting alternation may be insufficient to allow the proppant dune to reach the equilibrium state (Yew and Weng, 2014), thus resulting in the discrete pattern of the predicted curve and vertical pressure variations between slugs. It is likely that the transition state of the proppant dune between two alternating injections influences the pressure substantially, also contributing to the errors for the cases with pressure-ascending trends (Fig. 6). This feature describing the transition state, however, is not reflected by any model we evaluate in this study.

(ii) Fracture propagation during proppant injection – The introduction of the velocity feature (describing the critical flow condition that drives the proppant to turn into branching fractures) enhances the prediction performance for Wells D_2 and E_2 (Fig. 6), implying that more complex fracture networks may be generated. The amplitudes of the pressure fluctuations shown in Fig. 6 are broadly larger than those observed in Fig. 5, which may be attributed to the development of branching or minor fractures. The random fracture propagation may cause unexpected pressure variation and thus extra prediction errors (Fig. 6).

(iii) Proppant transport in highly-filled fractures – According to the discrepancies between reference and predicted DDP curves, the largest errors emerge at the beginning and end of proppant injections (Fig. 6). Initially, the fracture is underdeveloped with limited volumes. At the end of operations, a large volume of proppant has been injected into the fractures. The similarity of these two conditions is that the fracture is highly filled due to the relative volumes of fractures and proppant. However, few relevant research works can be found during our literature review. The highly-filled-fracture operating condition may be critical for pressure-sensitive cases and the sand screen-out, thus deserving more studies.

Therefore, we suggest investigating further (1) the evolution of proppant dune based on a staged pumping schedule, and (2) a better assessment of proppant transport in fracture networks and highly-filled

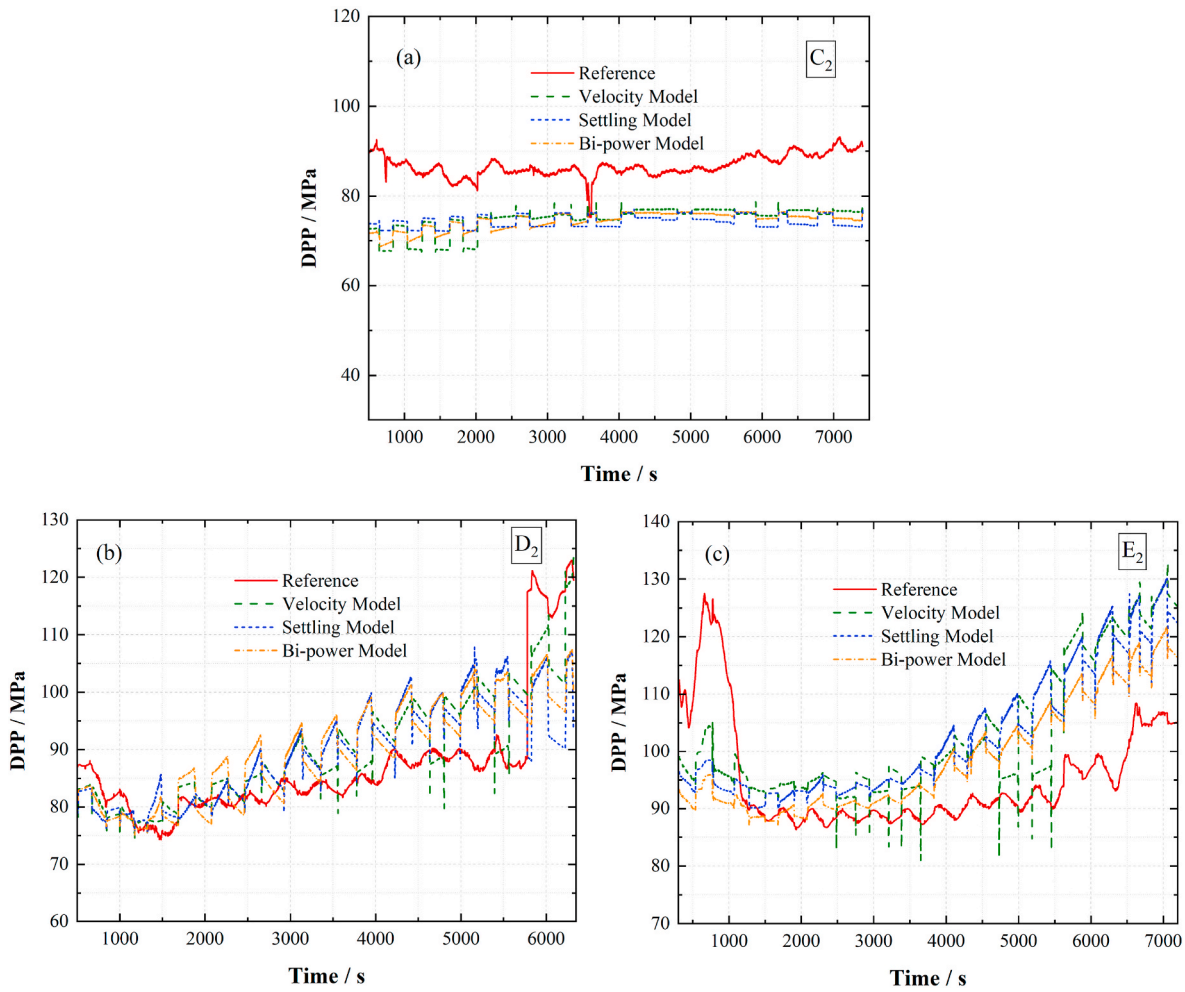

Fig. 6. Comparisons of the pressure evolution based on (a) well C_2, (b) well D_2 and (c) well E_2 using the GRU algorithm. The Reference curve (red solid line) is obtained by pressure conversion. The dashed lines are the proppant-transport-model-based predictions.

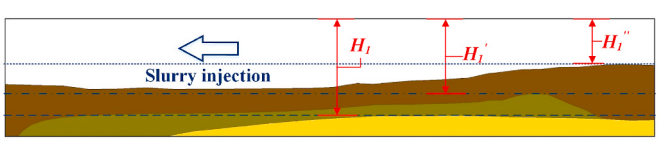

Fig. 7. Schematic of proppant accumulation in the fracture with slurry injection. The height of the flowing channel is decreased from H_1 to H_1', and then H_1''. The corresponding flowing resistance in the fracture increases with the decreasing height of the channel, thus fluctuating the wellhead pressure.

fractures.

5. Conclusions

In this study, we propose a machine-learning-based (GRU and SVM) workflow to process field measurements collected from shale gas fracturing to assess the essential proppant transport features and their corresponding calculations at field-practical scales. The features of particle settlement, stratified flow and inception are evaluated indirectly *via* algorithm training, fracturing pressure prediction and error analysis. The new workflow paves a path to potentially establish a link between laboratory work and engineering practices. The feature analysis improves the awareness of underground proppant transport in engineering scales, which may provide a complement to numerical and experimental simulations. The main conclusions are generalized as follows:

(1) The Bi-power model produces the most accurate prediction of fracturing pressures, followed by the Settling model (stratified-flow feature) and Velocity model (settlement and inception features). The introduction of the essential features enhances the pressure predictions for the cases where relatively flat trends of pressure evolution (under constant pump rates) are present, implying that the proppant is likely injected into a sufficient volume of fracture, comparable to the conditions simulated by the lab research.

(2) For the cases, where an ascending trend of pressure is shown throughout the proppant injections, all features and calculations bring in relatively large prediction errors. However, the Velocity model (characterizing the critical flow velocity that drives proppant to turn into branching fractures) helps to yield less prediction error in these cases, indicating that the proppant may be transported into un-fully-developed fracture networks. The underground fracture may be more complex in the pressure-ascending cases according to the more severely fluctuated pressure that may be induced by the generations of branching or minor fractures.

(3) The existing errors in the pressure-ascending cases can be improved by enhancing the accuracy of feature calculating models, where the alternate injection schedule and the random propagation of fracture are still missing. Based on the feature tests at field scales, we suggest that the evolution of proppant dune during an alternate pumping schedule may play a critical

role in pressure evolutions. Moreover, the proppant transport in fracture networks and highly-filled fractures should be defined more accurately for the pressure-sensitive operations to mitigate the operating risk and improve the proppant injection.

Credit author statement

Lei Hou: Conceptualization, Methodology, Investigation, Writing, Data Curation; **Xiaoyu Wang**: Methodology, Writing - Review & Editing; **Xiaobing Bian**: Investigation, Data Curation; **Honglei Liu**: Investigation, Data Curation; **Peibin Gong**: Writing - Review & Editing.

Declaration of competing interest

The authors declare that they have no known competing financial interests or personal relationships that could have appeared to influence the work reported in this paper.

Data availability

The authors do not have permission to share data.

Acknowledgement

This research has received funding from the European Union's Horizon 2020 research and innovation programme under the Marie Sklodowska-Curie grant agreement No. 846775.

Appendix A. Calculations used for pressure conversion

The original wellhead pressure (or surface pressure) is converted into downhole pressure to remove noises of flowing resistance and hydrostatic pressure variation caused by changes of pump rate, fluid type, proppant type and concentration.

$$P_{downhole} = P_{wellhead} + P_{statics} - P_{pipeloss} - P_{perforation} \tag{I}$$

The hydrostatic pressure ($P_{statics}$) is calculated by the vertical well depth (h_v)

$$P_{statics} = \rho_s g h_v \tag{II}$$

The friction loss of the wellbore ($P_{pipeloss}$) is estimated by the Darcy-Weisbach equation

$$P_{pipeloss} = 2f\frac{\rho_s {\upsilon_s}^2 L}{h_v} \qquad f = 0.046\left(\frac{\rho_s \upsilon_s h_v}{\mu_s}\right)^{-0.2} \tag{III}$$

where L is the wellbore length from its wellhead to the fracturing stage, m; υ_s is the flowing rate of slurry in the wellbore, m/s; μ_s is the slurry viscosity, Pa·s. The slurry viscosity is calculated by (Dontsov and Peirce, 2014)

$$\mu_s = \mu_f\left[\frac{5}{2}C_m A^{-1} + \left(0.32 + \frac{0.38}{1 + 5\times 10^{-5}A^{-2}}\right)A^{-2}\right] \qquad A = \frac{C_m}{C} - 1 \tag{V}$$

where C_m is the maximum proppant concentration and is assigned a value of 0.585.

The pressure drop through the perforation hole is estimated based on the hydraulic and perforation parameters (Willingham et al., 1993)

$$P_{perforation} = \frac{2.233\times 10^{-4} Q^2 \rho_s}{n^2 {d_h}^4 {C_p}^2} \tag{VI}$$

where d_h is the diameter of the perforation hole, m; C_p is the coefficient of discharge and is 0.6–0.95 for slurry; n is the number of the opening perforation hole. According to the mini-fracturing test, around half of the designed perforation holes will be opened.

Appendix B. Summary of feature calculations

1 Velocity model

The slickwater, widely used for massive hydraulic fracturing, could only suspend the proppant for minutes during the fracturing operation (Yew and Weng, 2014). Therefore, the proppant settling velocity, one of the most fundamental issues, is given by (Mack et al., 2014; McCabe et al., 1993)

$$\upsilon_{settling} = \left[\frac{0.072g(\rho_p - \rho_f)d^{1.6}}{\rho_f^{0.4}\mu_f^{0.6}}\right]^{0.71} \tag{1}$$

where $\upsilon_{settling}$ is the proppant settling velocity, m/s; ρ_p and ρ_f are densities of proppant and fracturing fluid, respectively, kg/m^3; μ_f is the fluid viscosity, Pa·s; d is the averaged diameter of proppant, m.

Settling in a fracture, proppant is slowed down by fracture walls and interactions between particles, which can be modified by (Gadde et al., 2004; Richardson and Zaki, 1954)

$$\begin{aligned} \upsilon'_{settling} &= \upsilon_{settling}\left(2.37C^2 - 3.08C + 1\right) \\ \upsilon''_{settling} &= \upsilon_{settling}\left[0.563\left(\frac{d}{w}\right)^2 - 1.563\frac{d}{w} + 1\right] \end{aligned} \tag{2}$$

where C is the volume fraction of proppant; w is the fracture width, m.

For a complex fracture network, the dragging of the carrying fluid is one of the most important motivations to drive the proppant turn into branch fractures (Rakshit Sahai et al., 2014). A minimum flowing rate of the slurry ($v_{turning}$) is required for proppant turning, and is estimated by the proppant restarting condition (Cao et al., 2006; Hou, Jiang, Li, et al., 2017a, 2017b)

$$v_{turning} = \frac{0.05(\rho_p - \rho_f)gdw}{8\mu_f} \tag{3}$$

The particle movements could reflect the proppant transporting by evaluating the ratio between particle and fluid velocities (Hou, Jiang, Li, et al., 2017a, 2017b). The Velocity model is defined as

$$\begin{cases} v_{settling}/v_f \\ v_{turning}/v_f \end{cases} \tag{4}$$

2 Settling model

The proppant is tending to form an equilibrium dune in low-viscosity fluids under constant injection conditions (Hou et al., 2019a, 2019b), as shown in Fig. 1 (b). The height of the flowing layer above the dune is a core parameter that evaluates the proppant transport. It could be estimated by the settling model expressed as (Novotny, 1977)

$$H_1 = \frac{16.67Q}{wv_{eq}} \tag{5}$$

where H_1 is the height of the flowing layer, m; Q is the pump rate, m^3/s; v_{eq} is the flowing rate when the particle settling and restarting reach equilibrium, and is calculated by

$$\begin{cases} v_{eq} = \left(\frac{(v_w)_{eq}}{0.2}\right)^{0.143} \frac{\left(2w\rho_f/\mu_f\right)^{0.143}}{\left(\rho_f/\rho_{SC}\right)^{0.571}} \\ (v_w)_{eq} = 18.5v_{Settling}\left(\frac{v_{Settling}d\rho_f}{\mu_f}\sqrt{\frac{2w}{d}}\right)^{-0.5} \\ \rho_s = \frac{\rho_f + \rho_p C(1-\varphi)}{1 + C(1-\varphi)} \end{cases} \tag{6}$$

where ρ_s is the density of the slurry, m^3/s; φ is the porosity of the proppant dune.

The slurry and pure fluid are usually injected alternately for shale gas fracturing. For the slurry condition, H_1 is estimated by Eq. (5). When pure fluid is injected, H_1 is assumed to be consistent with prior H_1 after the last slurry was injected. This process is carried out manually during the data pre-processing.

3 Bi-power model

The Bi-power law correlations are proposed to directly calculate the height of the flowing layer (Jing Wang et al., 2003), which is defined as

$$\frac{H_1}{w} = [-0.00023\ \ln(R_G) + 0.00292]R_f^{1.2-0.00126\lambda^{-0.428}[15.2-\ln(R_G)]}R_P^{[-0.0172\ \ln(R_G)-0.12]} \tag{7}$$

where R_f, R_p, R_G and λ are calculated by

$$\begin{cases} R_f = \frac{\rho_f Q_f}{w\mu_f} & R_p = \frac{\rho_p Q_p}{w\mu_f} \\ R_G = \frac{\rho_f(\rho_p - \rho_f)gd^3}{{\mu_f}^2} & \lambda = \frac{\mu_f/\rho_f}{w^{1.5}\sqrt{g}} \end{cases} \tag{8}$$

where Q_f is the pump rate of fracturing fluid, m^3/s; Q_p is the pump rate of proppant, m^3/s.

There is a special condition when pure fluid is injected to push the injected proppant deeply into the fracture. The pure fluid may rebalance the proppant dune, which could be calculated by (Patankar et al., 2002)

$$H_1 = \left(\frac{Q_f\rho_f w^{0.0937}}{2053.4\mu_f}\right)^{\frac{1}{1.0937}} \tag{9}$$

4 EDL model

A similar empirical power-law formula for dune height has been derived based on a series of sand-carrying experiments (Alotaibi and Miskimins, 2019). The equilibrium dune level (*EDL*) is defined as the dune height divided by fracture height, which is proposed as

$$EDL = -0.003496d^{-0.3277}\left[\frac{v_{eq}^{\left(0.7749^{-0.1955}\right)}}{C}\right] + 0.9901d^{-0.02667} \tag{10}$$

References

Al-Anazi, A., Gates, I., 2010. A support vector machine algorithm to classify lithofacies and model permeability in heterogeneous reservoirs. Eng. Geol. 114 (3–4), 267–277.

Al-Mudhafar, W.J., 2017. Multiple–point geostatistical lithofacies simulation of fluvial sand–rich depositional environment: a case study from zubair formation/South rumaila oil field. SPE Reservoir Eval. Eng. 21 (1), 39–53. https://doi.org/10.2118/187949-pa.

Alotaibi, M., Miskimins, J., 2019. Power law correlation for slickwater proppant dune height. In: Paper Presented at the SPE Hydraulic Fracturing Technology Conference and Exhibition.

Barboza, B.R., Chen, B., Li, C., 2021. A review on proppant transport modelling. J. Petrol. Sci. Eng. 204 https://doi.org/10.1016/j.petrol.2021.108753.

Barree, R., Conway, M., 1994. Experimental and numerical modeling of convective proppant transport. In: Paper Presented at the SPE Annual Technical Conference and Exhibition.

Ben, Y., Perrotte, M., Ezzatabadipour, M., Ali, I., Sankaran, S., Harlin, C., Cao, D., 2020. Real time hydraulic fracturing pressure prediction with machine learning. In: Paper Presented at the SPE Hydraulic Fracturing Technology Conference and Exhibition.

Cai, X., Guo, B., Li, G., Yang, X., 2017. A semi analytical model for predicting proppant screen-out during hydraulic fracturing unconventional reservoirs. In: Paper Presented at the SPE/IATMI Asia Pacific Oil & Gas Conference and Exhibition.

Cao, Z., Pender, G., Meng, J., 2006. Explicit formulation of the Shields diagram for incipient motion of sediment. J. Hydraul. Eng. 132 (10), 1097–1099.

Cho, K., Van Merriënboer, B., Gulcehre, C., Bahdanau, D., Bougares, F., Schwenk, H., Bengio, Y., 2014. Learning Phrase Representations Using RNN Encoder-Decoder for Statistical Machine Translation arXiv preprint arXiv:1406.1078.

Dahi-Taleghani, A., Olson, J.E., 2011. Numerical modeling of multistranded-hydraulic-fracture propagation: accounting for the interaction between induced and natural fractures. SPE J. 16 (3), 575–581.

Dontsov, E.V., Peirce, A.P., 2014. Slurry flow, gravitational settling and a proppant transport model for hydraulic fractures. J. Fluid Mech. 760, 567–590. https://doi.org/10.1017/jfm.2014.606.

Economides, M.J., Nolte, K.G., 1989. Reservoir Stimulation, vol. 2. Prentice Hall, Englewood Cliffs, NJ.

Elliott, S.J., Gale, J.F.W., 2018. Analysis and distribution of proppant recovered from fracture faces in the HFTS slant core drilled through a stimulated reservoir. In: Paper Presented at the Proceedings of the 6th Unconventional Resources Technology Conference.

Fan, D., Sun, H., Yao, J., Zhang, K., Yan, X., Sun, Z., 2021. Well production forecasting based on ARIMA-LSTM model considering manual operations. Energy 220. https://doi.org/10.1016/j.energy.2020.119708.

Fan, L., Thompson, J.W., Robinson, J.R., 2010. Understanding gas production mechanism and effectiveness of well stimulation in the Haynesville Shale through reservoir simulation. In: Paper Presented at the Canadian Unconventional Resources and International Petroleum Conference.

Gadde, P.B., Liu, Y., Norman, J., Bonnecaze, R., Sharma, M.M., 2004. Modeling proppant settling in water-fracs. In: Paper Presented at the SPE Annual Technical Conference and Exhibition.

Gal, Y., Ghahramani, Z., 2015. A Theoretically Grounded Application of Dropout in Recurrent Neural Networks arXiv preprint arXiv:1512.05287.

Goel, P., Saurabh, K., Patil-Shinde, V., Tambe, S.S., 2017. Prediction of API values of crude oils by use of saturates/aromatics/resins/asphaltenes analysis: computational-intelligence-based models. SPE J. 22 (3), 817–853.

Guo, Z., Chen, C., Gao, G., Cao, R., Li, R., Liu, H., 2018. Integration of support vector regression with distributed Gauss-Newton optimization method and its applications to the uncertainty assessment of unconventional assets. SPE Reservoir Eval. Eng. 21 (4), 1,007–1,026.

Hou, B., Chang, Z., Fu, W., Muhadasi, Y., Chen, M., 2019a. Fracture initiation and propagation in a deep shale gas reservoir subject to an alternating-fluid-injection hydraulic-fracturing treatment, 1 SPE J. 24 (4), 839, 831,855.

Hou, L., Bian, X., Geng, X., Sun, B., Liu, H., Jia, W., 2019b. Incipient motion behavior of the settled particles in supercritical CO2. J. Nat. Gas Sci. Eng. 68 https://doi.org/10.1016/j.jngse.2019.102900.

Hou, L., Cheng, Y., Wang, X., Ren, J., Geng, X., 2022. Effect of slickwater-alternate-slurry injection on proppant transport at field scales: a hybrid approach combining experiments and deep learning. Energy 242. https://doi.org/10.1016/j.energy.2021.122987.

Hou, L., Jiang, T., Li, G., Zeng, Y., Cheng, Y., 2017a. The key parameters of proppant transport in complex fractures. Chin. Sci. Bull. 62 (26), 3112–3120. https://doi.org/10.1360/n972016-00814.

Hou, L., Jiang, T., Liu, H., Geng, X., Sun, B., Li, G., Meng, S., 2017b. An evaluation method of supercritical CO2 thickening result for particle transporting. J. CO2 Util. 21, 247–252. https://doi.org/10.1016/j.jcou.2017.07.023.

Hu, J., Khan, F., Zhang, L., Tian, S., 2020. Data-driven early warning model for screenout scenarios in shale gas fracturing operation. Comput. Chem. Eng. 143 https://doi.org/10.1016/j.compchemeng.2020.107116.

Isah, A., Hiba, M., Al-Azani, K., Aljawad, M.S., Mahmoud, M., 2021. A comprehensive review of proppant transport in fractured reservoirs: experimental, numerical, and field aspects. J. Nat. Gas Sci. Eng. 88 https://doi.org/10.1016/j.jngse.2021.103832.

Kingma, D.P., Ba, J., 2014. Adam: A Method for Stochastic Optimization arXiv preprint arXiv:1412.6980.

Liang, F., Sayed, M., Al-Muntasheri, G.A., Chang, F.F., Li, L., 2016. A comprehensive review on proppant technologies. Petroleum 2 (1), 26–39.

Mack, M., Sun, J., Khadilkar, C., 2014. Quantifying proppant transport in thin fluids: theory and experiments. In: Paper Presented at the SPE Hydraulic Fracturing Technology Conference.

Manchanda, R., Zheng, S., Hirose, S., Sharma, M.M., 2020. Integrating reservoir geomechanics with multiple fracture propagation and proppant placement. SPE J. 25 (02), 662–691.

Mao, S., Zhang, Z., Chun, T., Wu, K., 2021. Field-scale numerical investigation of proppant transport among multicluster hydraulic fractures. SPE J. 26 (1), 307–323.

McCabe, W.L., Smith, J.C., Harriott, P., 1993. Unit Operations of Chemical Engineering, vol. 5. McGraw-hill, New York.

Nassir, M., Settari, A., Wan, R.G., 2014. Prediction of stimulated reservoir volume and optimization of fracturing in tight gas and shale with a fully elasto-plastic coupled geomechanical model. SPE J. 19 (5), 771–785.

Novotny, E., 1977. Proppant transport. In: Paper Presented at the SPE Annual Fall Technical Conference and Exhibition.

Patankar, N.A., Joseph, D., Wang, J., Barree, R., Conway, M., Asadi, M., 2002. Power law correlations for sediment transport in pressure driven channel flows. Int. J. Multiphas. Flow 28 (8), 1269–1292.

Richardson, J., Zaki, W., 1954. The sedimentation of a suspension of uniform spheres under conditions of viscous flow. Chem. Eng. Sci. 3 (2), 65–73.

Sahai, R., Miskimins, J.L., Olson, K.E., 2014. Laboratory results of proppant transport in complex fracture systems. In: Paper Presented at the SPE Hydraulic Fracturing Technology Conference.

Sahai, R., Moghanloo, R.G., 2019. Proppant transport in complex fracture networks–A review. J. Petrol. Sci. Eng. 182, 106199.

Sun, J.J., Battula, A., Hruby, B., Hossaini, P., 2020. Application of both physics-based and data-driven techniques for real-time screen-out prediction with high frequency data. In: Paper Presented at the Proceedings of the 8th Unconventional Resources Technology Conference.

Tong, S., Mohanty, K.K., 2016. Proppant transport study in fractures with intersections. Fuel 181, 463–477. https://doi.org/10.1016/j.fuel.2016.04.144.

Wang, J., Joseph, D.D., Patankar, N.A., Conway, M., Barree, R.D., 2003. Bi-power law correlations for sediment transport in pressure driven channel flows. Int. J. Multiphas. Flow 29 (3), 475–494.

Wang, J., Yan, J., Li, C., Gao, R.X., Zhao, R., 2019. Deep heterogeneous GRU model for predictive analytics in smart manufacturing: application to tool wear prediction. Comput. Ind. 111, 1–14. https://doi.org/10.1016/j.compind.2019.06.001.

Wei, G., Babadagli, T., Huang, H., Hou, L., Li, H., 2020. A visual experimental study: resin-coated ceramic proppants transport within rough vertical models. J. Petrol. Sci. Eng. 191 https://doi.org/10.1016/j.petrol.2020.107142.

Willingham, J., Tan, H., Norman, L., 1993. Perforation friction pressure of fracturing fluid slurries. In: Paper Presented at the Low Permeability Reservoirs Symposium.

Yew, C.H., Weng, X., 2014. Mechanics of Hydraulic Fracturing. Gulf Professional Publishing.

Yu, X., Trainor-Guitton, W., Miskimins, J., 2020. A data driven approach in screenout detection for horizontal wells. In: Paper Presented at the SPE Hydraulic Fracturing Technology Conference and Exhibition.

Zhang, G., Gutierrez, M., Li, M., 2017. Numerical simulation of transport and placement of multi-sized proppants in a hydraulic fracture in vertical wells. Granul. Matter 19 (2). https://doi.org/10.1007/s10035-017-0718-5.

Zhao, L., Chen, Y., Du, J., Liu, P., Li, N., Luo, Z., Huang, F., 2019. Experimental Study on a new type of self-propping fracturing technology. Energy 183, 249–261. https://doi.org/10.1016/j.energy.2019.06.137.